also conceivable that either some gaseous H_2CO_3 or solid H_2CO_3 on fine particles escapes into the stratosphere. Carbon dioxide is chemically inert in the troposphere and stratosphere (*40*). This might be different for (gaseous or solid) H_2CO_3 because its formation from CO_2 and H_2O is highly endergonic (*1–5*, *15*).

Further studies of gaseous H_2CO_3 should concentrate on its mass-spectral and spectroscopic characterization, and on the effects of temperature, vapor pressure, and water vapor on its kinetic stability. These data are essential to the search for gaseous and solid H_2CO_3 in future space missions.

REFERENCES AND NOTES

1. Literature up to 1973 is reviewed in *Gmelin Handbuch der Anorganischen Chemie, Kohlenstoff*, E. H. E. Pietsch and A. Kotowski, Eds. (Teil C3, Verlag Chemie, Weinheim, Germany, 1973), vol. 14, pp. 117–154; D. M. Kern, *J. Chem. Educ.* **37**, 14 (1960); M. Eigen, K. Kustin, G. Maass, *Z. Phys. Chem.* **30**, 130 (1961); Y. Pocker and D. W. Bjorkquist, *J. Am. Chem. Soc.* **99**, 6537 (1977); M. T. Nguyen and T.-K. Ha, *ibid.* **106**, 599 (1984).
2. B. Jönsson *et al.*, *J. Am. Chem. Soc.* **99**, 4628 (1977).
3. R. K. Khanna, J. A. Tossell, K. Fox, *Icarus* **112**, 541 (1994).
4. C. A. Wight and A. I. Boldyrev, *J. Phys. Chem.* **99**, 12125 (1995).
5. M. T. Nguyen, G. Raspoet, L. G. Vanquickenborne, P. Th. Van Duijnen, *J. Phys. Chem. A* **101**, 7379 (1997).
6. M. H. Moore and R. K. Khanna, *Spectrochim. Acta* **47 A**, 255 (1991).
7. ______, B. Donn, *J. Geophys. Res.* **96**, 17541 (1991).
8. N. DelloRusso, R. K. Khanna, M. H. Moore, *ibid.* **98**, 5505 (1993).
9. J. R. Brucato, M. E. Palumbo, G. Strazzulla, *Icarus* **125**, 135 (1997).
10. W. Hage, A. Hallbrucker, E. Mayer, *J. Am. Chem. Soc.* **115**, 8427 (1993).
11. ______, *J. Chem. Soc. Faraday Trans.* **91**, 2823 (1995).
12. ______, *ibid.* **92**, 3183 (1996).
13. ______, *ibid.*, p. 3197.
14. ______, *J. Mol. Struct.* **408/409**, 527 (1997).
15. K. R. Liedl, S. Sekušak, E. Mayer, *J. Am. Chem. Soc.* **119**, 3782 (1997).
16. J. K. Terlouw, C. B. Lebrilla, H. Schwarz, *Angew. Chem. Intl. Ed. Engl.* **26**, 354 (1987); J. K. Terlouw, D. Sülzle, H. Schwarz, *Angew. Chem.* **102**, 431 (1990).
17. The rate of sublimation at 200 K was determined by measuring the percent decrease of band areas of several selected bands of α-H_2CO_3 centered at 1713, 1328/1308, 1086, and 802 cm^{-1}. For a given time, percent decrease of the four bands was the same within $\pm$1% of relative band areas. The amount of sublimated H_2CO_3 was determined in an indirect way by comparing band areas of the composite D_2CO_3 band centered at ~1712 cm^{-1} (ν C = O) with that of the educt band in $KDCO_3$ centered at 1632 cm^{-1} (ν C = O) (*10*). For this comparison, spectra depicted in figure 1b of (*10*) as curves 1 and 5 for reaction in deuterated solution were selected, first, because in deuterated solution, the $KDCO_3$ band at 1632 cm^{-1} does not contain contributions from other bands (for example, the O-H deformation mode), and second, because the 1:1 correspondence between D_2CO_3 and DCO_3^- was established by quantitative conversion and the absence of enclosed CO_2. Band-area ratio was 0.33 for ν C = O (in D_2CO_3)/ν C = O (in DCO_3^-). In a next step, absorbance of the $KHCO_3$ band was determined in a calibrated liquid cell (15.0-μm path length) for 0.10 M $KHCO_3$ dissolved in methanol. This enabled us to determine via the band-area ratio the amount of sublimated H_2CO_3. At 200 K, the rate of H_2CO_3 sublimation was 1.10^{-8} cm^{-2} s^{-1} in this experiment.
18. W. Umrath, *Mikroskopie* **40**, 9 (1983).
19. R. C. Millikan and K. S. Pitzer, *J. Am. Chem. Soc.* **80**, 3515 (1958); T. Miyazawa and K. S. Pitzer, *J. Chem. Phys.* **30**, 1076 (1959); J. E. Bertie and K. H. Michaelian, *ibid.* **76**, 886 (1982); K. I. Lazaar and S. H. Bauer, *J. Am. Chem. Soc.* **107**, 3769 (1985); Y.-T. Chang, Y. Yamaguchi, W. H. Miller, H. F. Schaefer III, *ibid.* **109**, 7245 (1987); G. Henderson, *J. Chem. Educ.* **64**, 88 (1987); I. Yokoyama, Y. Miwa, K. Machida, *J. Am. Chem. Soc.* **113**, 6458 (1991).
20. G. Strazzulla, J. R. Brucato, G. Cimino, M. E. Palumbo, *Planet. Space Sci.* **44**, 1447 (1996).
21. D. Krankowsky *et al.*, *Nature* **321**, 326 (1986); J. Maddox, *ibid.*, p. 366; J. Crovisier *et al.*, *Astron. Astrophys.* **315**, L385 (1996).
22. A. H. Delsemme and P. Swings, *Ann. Astrophys.* **15**, 1 (1952); A. H. Delsemme and D. C. Miller, *Planet. Space Sci.* **18**, 709 (1970); *ibid.*, p. 717; S. L. Miller, in *Physics and Chemistry of Ice*, E. Whalley *et al.*, Eds. (Royal Society of Canada, Ottawa, 1973), pp. 42–50; J. I. Lunine and D. J. Stevenson, *Astrophys. J. Suppl. Ser.* **58**, 493 (1985); S. Engle, J. I. Lunine, J. S. Lewis, *Icarus* **85**, 380 (1990); A. Hallbrucker and E. Mayer, *ibid.* **90**, 176 (1991); D. Blake, L. Allamandola, S. Sandford, D. Hudgins, F. Freund, *Science* **254**, 548 (1991).
23. D. W. Davidson *et al.*, *J. Incl. Phenom.* **2**, 231 (1984).
24. Ch. Chyba and C. Sagan, *Nature* **330**, 350 (1987).
25. R. E. Johnson and T. I. Quickenden, *J. Geophys. Res.* **102**, 10985 (1997); K. Roessler, in *Handbook of Hot Atom Chemistry*, J. P. Adloff, Ed. (Kodansha, Tokyo, 1992), pp. 601–624.
26. M. Combes *et al.*, *Nature* **321**, 266 (1986).
27. M. Combes *et al.*, *Icarus* **76**, 404 (1988).
28. W. Calvin and T. Z. Martin, *J. Geophys. Res.* **99**, 21143 (1994).
29. R. P. Wayne, *Chemistry of the Atmospheres* (Clarendon Press, Oxford, 1995), chaps. 8 and 9.
30. L. C. Simonsen and J. E. Nealy, *NASA Tech. Paper* 3300 (1993).
31. T. B. McCord *et al.*, *Science* **278**, 271 (1997).
32. J. M. Greenberg and L. B. D'Hendecourt, in *Ices in the Solar System*, J. Klinger, D. Benest, A. Dollfus, R. Smoluchowski, Eds. (NATO ASI Series C 156, Reidel, Boston, MA, 1985), pp. 185–204; J. M. Greenberg, C. E. P. M. van de Bult, L. J. Allamandola, *J. Phys. Chem.* **87**, 4243 (1983).
33. For review see: E. Herbst, *Annu. Rev. Phys. Chem.* **46**, 27 (1995).
34. D. C. B. Whittet *et al.*, *Astron. Astrophys.* **315**, L357 (1996).
35. E. F. van Dishoeck *et al.*, *ibid.*, p. L349.
36. Th. de Graauw *et al.*, *ibid.*, p. L345.
37. K. Sassen, K. N. Liou, S. Kinne, M. Griffin, *Science* **227**, 411 (1985); K. Sassen, *ibid.* **257**, 516 (1992).
38. W. Stumm and J. J. Morgan, *Aquatic Chemistry* (Wiley-Interscience, New York, 1996), pp. 206–249.
39. G. P. Ayers, R. W. Gillett, E. R. Caeser, *Tellus B* **37**, 35 (1985).
40. M. J. Molina, L. T. Molina, Ch. E. Kolb, *Annu. Rev. Phys. Chem.* **47**, 327 (1996).
41. Infrared spectra were recorded in transmission on Biorad's FTS 45 at 2 cm^{-1} resolution (DTGS detector, UDR1) by coadding 50 scans. The spectrum of water vapor was subtracted from the spectra.

42. We are grateful to S. Sekušak for help in the early stages of the calculations and to the Forschungsförderungsfonds of Austria for financial support (project P12319-PHY).

26 September 1997; accepted 21 January 1998

Abrupt Climate Events 500,000 to 340,000 Years Ago: Evidence from Subpolar North Atlantic Sediments

D. W. Oppo, J. F. McManus, J. L. Cullen

Subpolar North Atlantic proxy records document millennial-scale climate variations 500,000 to 340,000 years ago. The cycles have an approximately constant pacing that is similar to that documented for the last glacial cycle. These findings suggest that such climate variations are inherent to the late Pleistocene, regardless of glacial state. Sea surface temperature during the warm peak of Marine Isotope Stage 11 (MIS 11) varied by 0.5° to 1°C, less than the 4° to 4.5°C estimated during times of ice growth and the 3°C estimated for glacial maxima. Coherent deep ocean circulation changes were associated with glacial oscillations in sea surface temperature.

During the last glaciation (MIS 2 to 4) and deglaciation, sea surface temperatures (SSTs) oscillated in the subpolar North Atlantic at several time scales. Discrete ice-rafting events marked times of cool SSTs. A series of gradual cooling intervals 6000 to 10,000 years (6 to 10 ky) long were terminated by massive iceberg discharge into the North Atlantic (Heinrich events) (*1–3*). Shorter SST cycles of 2 to 3 ky [Dansgaard-Oeschger cycles (*4*)], each terminated by a cold ice-rafting event, occurred between Heinrich events (*5*). New evidence indicates that there may have been more frequent sea surface changes, spaced ~1.5 ky apart (*6*). A similar hierarchy is emerging from Greenland ice core records: glaciochemical time series indicate that the strength of the polar atmospheric circulation varied over cycles of between 6 and 1.45 ky (*7*), comparable to the approximate spacing of events deduced from the marine record. Such millennial climate oscillations also occurred during the Holocene (*6–8*).

Deep-water circulation variability may

D. W. Oppo and J. F. McManus, Department of Geology and Geophysics, Woods Hole Oceanographic Institution, Woods Hole, MA 02543, USA.
J. L. Cullen, Department of Geological Sciences, Salem State College, Salem, MA 01970, USA.

play a critical role in driving and amplifying millennial climate oscillations (6, 9), as well as communicating the response outside of the North Atlantic (10). Cold glacial events were often associated with weakened production of North Atlantic Deep Water (NADW) (11–14).

The finding of similar cycles during glacial times and the Holocene (MIS 1) suggest that they characterize Earth's climate system independent of ice volume. If this is true, then older sediments should reveal millennial-scale climate oscillations at a similar pacing. Indeed, ice-rafting events every 2 to 3 ky have been identified in glacial intervals of the early Pleistocene (13), a time when climate varied at the 40-ky obliquity cycle (15) and ice sheets were about one-quarter to two-thirds the size of those of the last glacial maximum (13).

To explore the persistence of a link between SST and deep-water millennial-scale variability throughout the Pleistocene, we studied sediments from Ocean Drilling Project site 980 on the Feni Drift (55.5°N, 14.7°W, 2179 m below sea level) (16), dated ~340 to 500 thousand years ago (ka) (17). By this time, late Pleistocene 100-ky climate cycles, characterized by rapid deglaciations, or terminations (18), were firmly established (15). This time interval includes MIS 12 and 11, which are among the most extreme glacial and interglacial intervals, respectively, of the past 500 ky (19). The associated deglaciation, Termination V, had a large amplitude even though insolation forcing was weaker than at the time of most other terminations (20). The interval includes two ice-growth transitions (13/12 and 11/10) that are comparable to MIS 3 through early MIS 2, the part of the last glacial cycle containing the highest amplitude millennial-scale variations (7, 21). We collected $\delta^{18}O$ and $\delta^{13}C$ records (22) of the benthic foraminifera *Cibicidoides wuellerstorfi* and $\delta^{18}O$ records of the planktonic foraminifera right-coiling *Neogloboquadrina pachyderma* (*N. pachy*-R $\delta^{18}O$) to provide detailed estimates of ice volume and deep-water circulation and to study surface water hydrography. The samples were spaced about 300 years apart.

At the Bjorn Drift, to the northwest of site 980, SST estimates across the MIS 6/5 boundary (Termination II) based on *N. pachy*-R $\delta^{18}O$ and the modern analog technique are similar (23), suggesting that *N. pachy*-R $\delta^{18}O$ more accurately record SST than the $\delta^{18}O$ of other high-latitude planktonic foraminifera (24). To further examine the extent to which *N. pachy*-R $\delta^{18}O$ records SST variations, we measured the percentage of the polar planktonic foraminifera left-coiling *N. pachyderma* (%*N. pachy*-L), a more widely used but qualitative proxy for SST, on the same samples in an 87-ky time slice (350 to 437 ka) that included peak MIS 12 through the early part of MIS 10. Lithic fragments, or ice-rafted debris, were also counted in the same time slice.

The proxy records (Fig. 1) exhibit millennial-scale variability superimposed on variability forced by slowly changing insolation. During the ice-growth transition between MIS 11 and 10, *N. pachy*-R $\delta^{18}O$ oscillated by 1 per mil, and %*N. pachy*-L varied over a 50% range (Fig. 2A). The amplitude of both of these signals corresponds to SST oscillations of about 4° to 4.5°C (25), suggesting that *N. pachy*-R $\delta^{18}O$ records the full range of SST oscillations during this transition. The agreement between the two proxies improves when the ice volume component of the *N. pachy*-R $\delta^{18}O$ signal is removed by subtracting the benthic $\delta^{18}O$ record (Fig. 2B). The %*N. pachy*-L record does not extend to the end of MIS 10, but *N. pachy*-R $\delta^{18}O$ oscillations through 340 ka imply that SST oscillations also occurred during MIS 10. Five of the six coldest events during the MIS 11/10 transition (events *c* through *g*) and one event within MIS 10 (event *b*) are associated with lithic evidence of iceberg discharge (Fig. 2C). In all, eight to nine strong coolings occurred within a 50-ky interval, for an average spacing of 6 ky, comparable to the spacing of Heinrich events during the last glacial cycle (1–3, 7, 26). Weaker cold events occurred more frequently. The spacing between severe cold events appears to have decreased with increasing ice volume. A series of gradual cooling intervals culminated in cold iceberg discharge events *g*, *f*, *d*, and *b*. Thus, the character of the climate signal is reminiscent of that of MIS 3 (2). Furthermore, as during the last glacial cycle

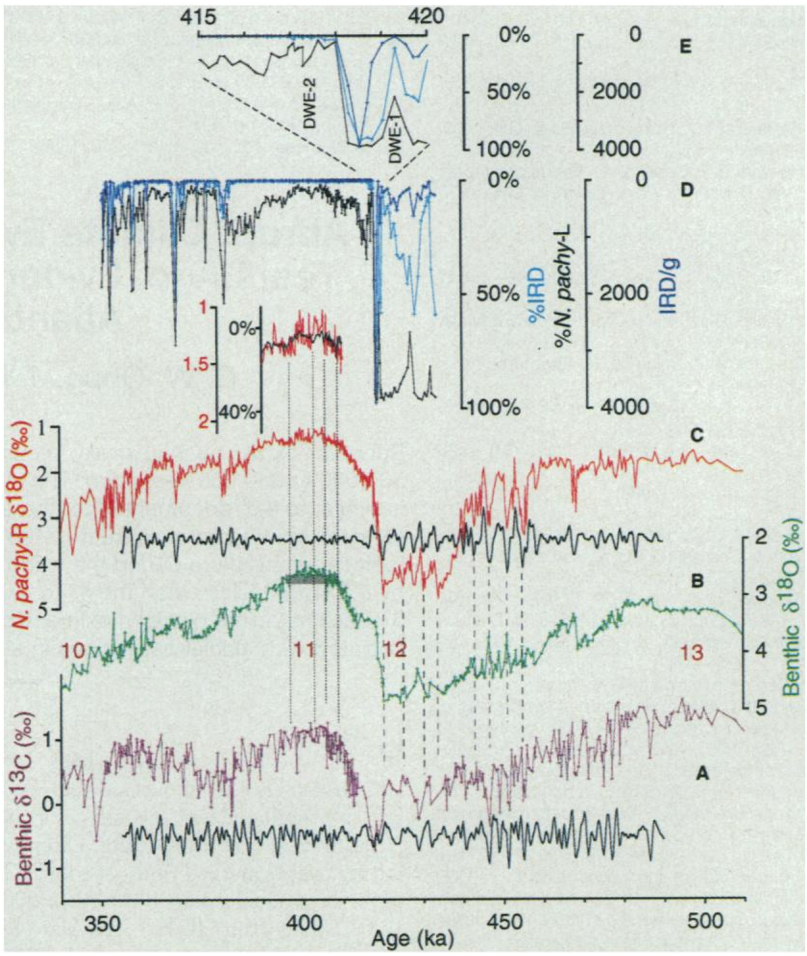

Fig. 1. Summary of site 980 data. (**A**) *C. wuellerstorfi* $\delta^{13}C$ values (‰, per mil), (**B**) *C. wuellerstorfi* $\delta^{18}O$ values, (**C**) *N. pachyderma* (right-coiling) $\delta^{18}O$ values, (**D**) lithic counts (ice-rafted debris) expressed as a percentage relative to total entities (%IRD, blue) and as a ratio relative to weight of dry bulk sediment (IRD/g, black), and (**E**) an enlarged version of the data in (D) for 415 to 420 ka. Deglacial warm events (DWE) are labeled. (A) and (C) also include the 1- to 7-ky bandpass filter (31) of the data (black). Shaded interval in (B) indicates the peak of MIS 11. Dashed and dotted lines denote times of cooler temperatures. Inset between (C) and (D) shows *N. pachy*-R $\delta^{18}O$ (red) and %*N. pachy*-L (black) scaled to equivalent temperature (25) for MIS 11.

(*11, 12*), the coldest events were generally associated with low benthic $\delta^{13}C$ values (Fig. 2C), implying that the contribution of high- $\delta^{13}C$ NADW to the site was reduced. Other $\delta^{13}C$ minima are associated with weaker cool events, which may have been more pronounced to the north of site 980.

During the MIS 13/12 ice-growth transition, *N. pachy*-R $\delta^{18}O$ oscillated by >1 per mil (Fig. 1C), indicating that SST oscillated by 4° to 4.5°C on this transition as well. Severe cold events occurred more frequently as ice volume increased. During the peak of MIS 12, $\delta^{18}O$ varied by ~0.75 per mil (~3°C), much less than during the two ice-growth transitions. Like cold events during the MIS 11/10 transition and during the last glacial cycle, cold events during the MIS 13/12 transition and within MIS 12 were associated with low benthic $\delta^{13}C$ values (Figs. 1 and 3), indicative of reduced NADW production (*27*). The lower amplitude of benthic $\delta^{13}C$ (deep water) variations within MIS 12 compared with those during the 11/10 and 13/12 transitions is consistent with recent modeling experiments that suggest that convective overturn in the North Atlantic is more oscillatory when freshwater discharge is moderate, as might occur during intervals of ice growth, than when discharge is high (maximum glacial) or low (interglacial) (*28*).

The end of MIS 12 is marked by a drop in benthic $\delta^{18}O$ (Fig. 1B) associated with sea-level rise at ~420 ka (*16*). A decrease in %*N. pachy*-L indicates that the beginning of sea-level rise was immediately followed by a brief deglacial warm event (DWE-1) (Fig. 1E). After DWE-1, a cold and severe ice-rafting event occurred. The presence of detrital carbonate suggests that it involved massive discharge from the Laurentide ice sheet, as did Heinrich events of Mis 2 and 3 (*2, 3*). Despite extreme cold, a decrease of ~0.4 per mil in benthic $\delta^{18}O$ (Fig. 1B) suggests that sea-level rise accelerated during the cold event. A decrease in %*N. pachy*-L and ice-rafted debris indicates that a second deglacial warm event (DWE-2) abruptly ended the Heinrich-like cold event (Fig. 1E). After DWE-2, which was itself punctuated by a brief cool event, %*N. pachy*-L rose to about 30%, indicating that a less severe cooling (2° to 3°C) occurred before the final warming into peak MIS 11.

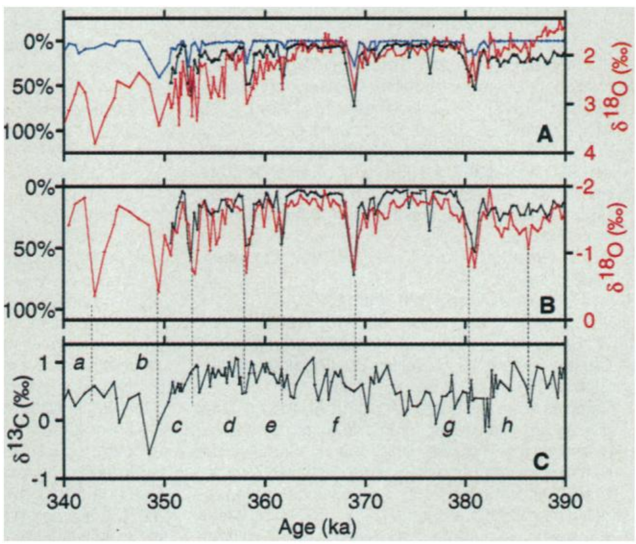

Fig. 2. (**A**) *N. pachy*-R $\delta^{18}O$ (red) and %*N. pachy*-L (black) scaled to equivalent temperature (*25*). Lithic count (%IRD as in Fig. 1) (blue, left axis) is also shown. (**B**) *N. pachy*-R $\delta^{18}O$ minus benthic $\delta^{18}O$ (red) versus %*N. pachy*-L (black) scaled to equivalent temperature. (**C**) Benthic $\delta^{13}C$ values. Severe cold and ice-rafting events are labeled.

After this last deglacial cold event, a decrease in *N. pachy*-R $\delta^{18}O$ and %*N. pachy*-L and an increase in benthic $\delta^{13}C$ (Fig. 1) indicate developing interglacial conditions, warming, and enhanced NADW production. Small oscillations in %*N. pachy*-L, *N. pachy*-R $\delta^{18}O$, and benthic $\delta^{13}C$ punctuated the gradual climatic amelioration into MIS 11. Variations of *N. pachy*-L abundance by ~5% suggest that SST oscillated by ~0.5°C. Although the *N. pachy*-R $\delta^{18}O$ data show more scatter, $\delta^{18}O$ variations of ~0.2 per mil suggest that SST varied by ~1°C. At the low *N. pachy*-L percentages measured (1 to 7%), the relation between SST and %*N. pachy*-L is weak (*29*); thus, the amplitude of SST variability within MIS 11 was likely closer to the 1°C estimated by the *N. pachy*-R $\delta^{18}O$ data. During the 10- to 12-ky interval of minimum ice volume (benthic $\delta^{18}O \leq$ 2.7 per mil) and maximum SSTs of peak MIS 11, three SST cycles are evident, giving a repeat time of 3 to 4 ky, comparable to cycles documented in marine and ice core records for the last 100 ky (*5, 7*). Although the benthic $\delta^{13}C$ data do not provide clear evidence that NADW was reduced during cool MIS 11 events, we cannot rule out this possibility because the site is close to the deep-water source region and may not be sensitive to subtle variations in NADW during peak interglacial intervals, when NADW production is generally strong.

Spectral analysis of %*N. pachy*-L, *N. pachy*-R $\delta^{18}O$, and benthic $\delta^{13}C$ records using Blackman-Tukey (*30*) methods confirm the presence of cycles (Fig. 3) with frequencies close to those noted in the glaciochemical record from the Greenland ice core and in the marine records for the last glacial cycle and the Holocene. For their interval of overlap (350 to 437 ka), the *N. pachy*-R $\delta^{18}O$ and %*N. pachy*-L records are coherent and in phase in broad bands centered near 6, 2.6, 1.8, and 1.4 ky (Fig. 3A). These relations further suggest the utility of *N. pachy*-R $\delta^{18}O$ as a SST proxy, in particular when changes in ice volume are minor. For their interval of overlap (350 to 437

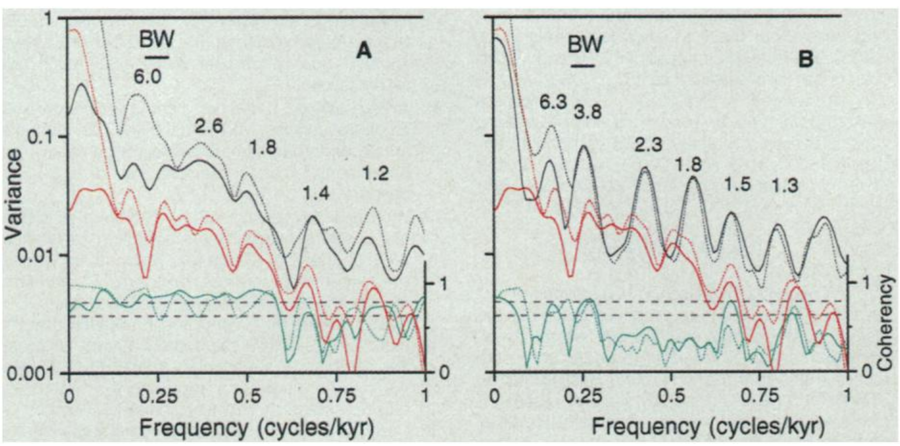

Fig. 3. Summary of spectral analysis. (**A**) Spectra of the %*N. pachy*-L (red) and *N. pachy*-R $\delta^{18}O$ (black) records. The green line shows the coherency between the two shorter records. Solid and dashed lines are results using the entire (to 437 ka, the length of the %*N. pachy*-L record) records and only 350 to 410 ka, respectively. The dashed horizontal lines are the 80% and 95% test statistics for non-zero coherency. (**B**) As in (A), except the black lines are spectra of benthic $\delta^{13}C$, and the green lines are the coherency between %*N. pachy*-L and benthic $\delta^{13}C$. Bandwidth (BW) is shown.

ka), the %*N. pachy*-L and benthic $\delta^{13}C$ records are coherent at periods near 6.3 and 3.8 ky. Power occurs in both records in broad bands centered near 2.3 and 1.8 ky; however, their coherence is weak (Fig. 3B). For the 350- to 410-ka interval (omitting the termination), variations near 1.5 ky are also coherent (Fig. 3B). Benthic $\delta^{13}C$ and %*N. pachy*-L changes are approximately in phase near the 6.3- and 1.5-ky periods, indicating that surface- and deep-water changes occurred together at these cycles. The in-phase behavior at the 6.3-ky period reflects the association of the larger millennial-scale SST minima, which occurred ~6 ky apart, with low benthic $\delta^{13}C$ values (Figs. 1 and 2). By contrast, SST changes began ~800 years after changes in NADW production near the 3.8-ky period. This phase difference accounts for some of the differences in timing of changes evident in the benthic $\delta^{13}C$ and %*N. pachy*-L records (Fig. 1).

We used a bandpass filter (*31*) to examine the amplitude of higher frequency (1 to 7 ky) variations in the *N. pachy*-R $\delta^{18}O$ values. The filtered signal underscores the small-amplitude millennial-scale variations during interglaciations MIS 11 and 13 relative to variations that characterized times of large ice volume or ice growth. Climate oscillations during deglaciation were part of the regular sequence of millennial-scale oscillations.

Our study indicates that variability in the climate from 350 to 500 ka was similar to that of the last glacial cycle, suggesting that millennial-scale variability persisted during the past half a million years. The amplitude of the variability was much smaller during interglacial intervals and greatest during ice growth. Severe events became more frequent near glacial maxima. The pacing of climatic events during our 150-ky-long core interval is indistinguishable from that during the last glacial cycle. Sea surface temperature and deep water varied together at a cycle near 6 ky. At shorter (3.8 and 1.5 ky) cycles, surface and deep-water changes occurred, on average, several hundred years apart. Our data suggest that variability in benthic $\delta^{13}C$ (deep water) values was also greater during ice-growth transitions, consistent with a role of deep water in amplifying millennial climate cycles (*6, 9, 28*).

REFERENCES AND NOTES

1. H. Heinrich, *Quat. Res.* **29**, 142 (1988).
2. G. Bond *et al.*, *Nature* **365**, 143 (1993).
3. W. S. Broecker, G. Bond, M. Klas, E. Clark, J. McManus, *Clim. Dyn.* **6**, 265 (1992).
4. W. Dansgaard *et al.*, in *Climate Processes and Climate Sensitivity*, J. E. Hansen and T. Takahashi, Eds. (American Geophysical Union, Washington, DC, 1984), vol. 5, pp. 288–298.
5. G. Bond and R. Lotti, *Science* **267**, 1005 (1995).
6. G. Bond *et al.*, *ibid.* **278**, 1257 (1997).
7. P. A. Mayewski *et al.*, *J. Geophys. Res.* **102**, 26345 (1997).
8. S. R. O'Brien *et al.*, *Science* **270**, 1962 (1995); L. D. Keigwin, *ibid.* **274**, 1504 (1996).
9. W. S. Broecker, G. Bond, M. Klas, G. Bonani, W. Wolfi, *Paleoceanography* **5**, 469 (1990).
10. U. Mikolajewicz, T. J. Crowley, A. Schiller, R. Voss, *Nature* **387**, 384 (1997).
11. L. D. Keigwin and G. A. Jones, *J. Geophys. Res.* **99**, 12397 (1994); L. Vidal *et al.*, *Earth Planet. Sci. Lett.* **146**, 13 (1997).
12. D. W. Oppo and S. J. Lehman, *Paleoceanography* **10**, 901 (1995).
13. M. E. Raymo, K. Ganley, S. Carter, D. W. Oppo, J. McManus, in preparation.
14. W. B. Curry and D. W. Oppo, *Paleoceanography* **12**, 1 (1997).
15. N. G. Pisias and T. C. Moore, *Earth Planet. Sci. Lett.* **52**, 450 (1981); W. F. Ruddiman, A. McIntyre, M. Raymo, *ibid.* **80**, 117 (1986); W. F. Ruddiman, M. E. Raymo, D. G. Martinson, B. M. Clement, J. Backman, *Paleoceanography* **4**, 353 (1989).
16. We used the time scale presented by N. J. Shackleton, A. Berger, and W. R. Peltier [*Trans. R. Soc. Edinburgh Earth Sci.* **81**, 25 (1990)].
17. Because of its high sedimentation rates and sensitive location just north of the glacial polar front, the Feni Drift has been the focus of many studies of suborbital-scale climate variability over the last glacial cycle [(*2, 3, 5, 6*); G. Bond *et al.*, *Nature* **360**, 245 (1992); J. F. McManus *et al.*, *ibid.* **371**, 326 (1994); E. Cortijo, P. Yiou, L. Labeyrie, M. Cremer, *Paleoceanography* **10**, 911 (1995); S. G. Robinson, M. Maslin, I. N. McCave, *ibid.*, p. 221; L. D. Labeyrie *et al.*, *Philos. Trans. R. Soc. London Ser. B* **348**, 255 (1995)]. ODP site 980 was drilled with the goal of extending the results from the last glacial cycle to earlier intervals. Sedimentation rates average 11 cm/ky over the study interval.
18. W. S. Broecker and J. V. Donk, *Rev. Geophys. Space Phys.* **8**, 169 (1970).
19. W. R. Howard, *Nature* **388**, 418 (1997).
20. A. L. Berger, *J. Atmos. Sci.* **35**, 2362 (1978).
21. W. Broecker, G. Bond, J. McManus, in *Ice in the Climate System*, W. R. Peltier, Ed. (Springer-Verlag, Berlin, 1993), vol. 12, pp. 161–166.
22. Samples were dry-sieved at 150 mm, then split to give ~300 planktonic foraminifera for *N. pachyderma* (left-coiling) and lithic counts. Samples for isotope analysis consisted of one to three *C. wuellerstorfi* specimens (>150 mm) or about seven *N. pachyderma* (right-coiling) (150 to 250 mm). Measurements were made at the Woods Hole Oceanographic Institution on a Finnigan MAT252 coupled to an automated carbonate preparation device consisting of 46 single-reaction chambers, with 23 chambers on each of two lines. Acid temperature was ~70°C. The isotopic compositions $\delta^{18}O$ and $\delta^{13}C$ in units of per mil are defined as $[(R_{sample}/R_{standard}) - 1] \times 10^3$, where $R = {}^{18}O/{}^{16}O$ and ${}^{13}C/{}^{12}C$, respectively. The standard deviation of the isotope values of National Bureau of Standards (NBS) carbonate standard NBS19 is 0.08 and 0.04 per mil for $\delta^{18}O$ and $\delta^{13}C$, respectively. Calibration to Pee Dee belemnite was done with NBS19 ($\delta^{18}O$ = −2.2 VPDB, $\delta^{13}C$ = 1.95 VPDB).
23. D. W. Oppo, M. Horowitz, S. J. Lehman, *Paleoceanography* **12**, 51 (1997).
24. The $\delta^{18}O$ record for right-coiling *N. pachyderma* varies across Termination II by ~1 per mil more than the glacial-interglacial change of both left-coiling *N. pachyderma* and *Globergerina bulloides* [compare record in (*23*) to those in (*12*)], suggesting that *N. pachy*-R $\delta^{18}O$ is less biased by changes in seasonality or depth-habitat than the records of the other two species. In the subpolar North Atlantic, surface salinities were probably lower during glacial than interglacial times [E. A. Boyle and L. D. Keigwin, *Nature* **330**, 35 (1987)]; thus, it is likely that glacial SSTs were lower than estimated from *N. pachy*-R $\delta^{18}O$. If true, the faunal estimates must also underestimate the full amplitude of the glacial-interglacial SST change.
25. Using a scaling of 1°C = 0.23 per mil in $\delta^{18}O$ [S. R. Epstein, R. Buchsbaum, H. A. Lowenstam, H. C. Urey, *Geol. Soc. Am. Bull.* **64**, 1315 (1953)] , the $\delta^{18}O$ oscillations of 1 per mil correspond to ~4.5°C. In the modern ocean, %*N. pachy*-L varies over an 8°C range [(*29*); A. W. H. Bé and D. S. Tolderlund, in *Micropaleontology of Oceans*, B. M. Funnell and W. R. Riedel, Eds. (Cambridge Univ. Press, London, 1971), pp. 105–149; T. B. Kellogg, *Boreas* **9**, 115 (1980)]. Because %*N. pachy*-L is not saturated at the 0 or 100% level, we can assume that a 50% change corresponds to about half of the 8°C range, qualitatively similar to the SST change estimated from *N. pachy*-R $\delta^{18}O$.
26. F. E. Grousset *et al.*, *Paleoceanography* **8**, 175 (1993).
27. During MIS 12, benthic $\delta^{13}C$ values were higher at site 980 than at deep North Atlantic DSDP site 607 (41°N, 33°W, 3427 m below sea level) {$\delta^{13}C \leq -0.5$ per mil [M. E. Raymo, W. F. Ruddiman, N. J. Shackleton, D. W. Oppo, *Earth Planet. Sci. Lett.* **97**, 353 (1990)]}. This difference suggests that at this time, high-$\delta^{13}C$ Glacial North Atlantic Intermediate Water (GNAIW) had replaced NADW as the primary northern deep-water mass, and the depth of site 980 (2179 m) was within GNAIW or within the sharp gradient between GNAIW and low-$\delta^{13}C$ deep water derived from the south [D. W. Oppo and S. J. Lehman, *Science* **259**, 1148 (1993)]. Coincident with benthic $\delta^{18}O$ evidence for sea-level rise ~420 ka, $\delta^{13}C$ values decreased at site 980, indicating that GNAIW shoaled and that site 980 also lay within the deeper water mass. At site 980, $\delta^{13}C$ values continued to decrease into the beginning of the DWE-1, but the absence of *C. wuellerstorfi* preclude measurements within the peak of DWE-1. The $\delta^{13}C$ values are low within DWE-2 and only began to rise in association with the warming out of the last cold event. With the existing (orbital-scale resolution) deep North Atlantic records, we cannot address whether the weakening of GNAIW was associated with strengthening of NADW, as has been documented for the last deglaciation (T. M. J. Marchitto, W. B. Curry, D. W. Oppo, in preparation). However, the decreasing strength of GNAIW associated with Termination V confirms that vertical water-mass reorganization is an important and persistent feature of deglaciations [M. Sarnthein and R. Tiedemann, *Paleoceanography* **5**, 1041 (1990)]. Water-mass restructuring, which results in an increase in heat release at high northern latitudes, has probably been one of the most important climatic feedbacks accelerating deglaciation [S. J. Lehman and L. D. Keigwin, *Nature* **356**, 757 (1992)].
28. K. Sakai and W. R. Peltier, *J. Clim.* **10**, 949 (1997).
29. K. E. Kohfield, R. G. Fairbanks, S. L. Smith, I. D. Walsh, *Paleoceanography* **11**, 679 (1996).
30. G. M. Jenkins and D. G. Watts, *Spectral Analysis and Its Applications* (Holden-Day, San Francisco, 1968). Multiple-taper methods [D. J. Thomson, *Philos. Trans. R. Soc. London Ser. A* **332**, 539 (1990)] gave similar results.
31. A zero-phase, 128-order Hamming window with cutoff frequencies 1/6.7 and 1/1 ky. The change in amplitude through time is similar for narrower pass bands centered at, for example, the 1.5- and 3.8-ky periods.

32. We thank S. Healy, L. Zou, T. Norris, D. Ostermann, and M. Jeglinski for laboratory assistance. We also thank A. Martin and R. Norris for lending their expertise on foramifer taxonomy, P. Howell for making the time series programs available, ODP, and co-chiefs M. Raymo and E. Jansen and the rest of the Leg 162 shipboard party for acquiring the samples. We especially thank T. C. E. van Weering for generously providing the site survey data for site 980. We also thank M. Raymo, W. Curry, and two reviewers for comments on the manuscript. This work was funded by NSF grant OCE-9632172 (D.W.O.), a Woods Hole Oceanographic Institution postdoctoral scholarship (J.F.M.), and a Joint Oceanographic Institutions–U.S. Science Advisory Committee grant (J.L.C.).

20 November 1997; accepted 16 January 1998